nature chemical biology

ARTICLE

PUBLISHED ONLINE: 29 AUGUST 2016 | DOI: 10.1038/NCHEMBIO.2165

Dual action antifungal small molecule modulates multidrug efflux and TOR signaling

Tanvi Shekhar-Guturja[1], G M Kamal B Gunaherath[2], E M Kithsiri Wijeratne[2], Jean-Philippe Lambert[3], Anna F Averette[4], Soo Chan Lee[4], Taeyup Kim[4], Yong-Sun Bahn[5], Farida Tripodi[6], Ron Ammar[7], Katja Döhl[8], Karolina Niewola-Staszkowska[9], Lutz Schmitt[8], Robbie J Loewith[9], Frederick P Roth[1,3], Dominique Sanglard[10], David Andes[11,12], Corey Nislow[13], Paola Coccetti[6], Anne-Claude Gingras[1,3], Joseph Heitman[4], A A Leslie Gunatilaka[2] & Leah E Cowen[1]*

There is an urgent need for new strategies to treat invasive fungal infections, which are a leading cause of human mortality. Here, we establish two activities of the natural product beauvericin, which potentiates the activity of the most widely deployed class of antifungal against the leading human fungal pathogens, blocks the emergence of drug resistance, and renders antifungal-resistant pathogens responsive to treatment in mammalian infection models. Harnessing genome sequencing of beauvericin-resistant mutants, affinity purification of a biotinylated beauvericin analog, and biochemical and genetic assays reveals that beauvericin blocks multidrug efflux and inhibits the global regulator TORC1 kinase, thereby activating the protein kinase CK2 and inhibiting the molecular chaperone Hsp90. Substitutions in the multidrug transporter Pdr5 that enable beauvericin efflux impair antifungal efflux, thereby impeding resistance to the drug combination. Thus, dual targeting of multidrug efflux and TOR signaling provides a powerful, broadly effective therapeutic strategy for treating fungal infectious disease that evades resistance.

© 2016 Nature America, Inc. All rights reserved.

Fungi have a staggering impact on human health. They infect billions of people worldwide and kill more than 1.5 million people per year[1]. The most vulnerable individuals are those whose immune systems are compromised due to chemotherapy, transplant of solid organs or hematopoietic stem cells, or infection with HIV. The frequency of invasive fungal infections has increased by more than 200% in recent decades, in keeping with the growing population of immunocompromised individuals[2]. The most deadly fungal pathogens are species of *Candida*, *Aspergillus,* and *Cryptococcus*. Despite state-of-the-art treatments, mortality rates from systemic fungal infections remain unacceptably high, varying from 30–95%, depending on the pathogen and patient population[1].

The armamentarium of antifungal drugs is sparse, with the efficacy of most agents being compromised by host toxicity, fungistatic activity, or drug resistance[3]. There are only three major classes of antifungals used for treatment of invasive fungal infections[2]. The polyenes, discovered over 60 years ago, exert fungicidal activity by extracting ergosterol from fungal cell membranes[4], often causing toxic side-effects in patients because of their impact on cholesterol in human cells. The azoles were introduced over 40 years ago and remain the most widely deployed antifungals[2]. They inhibit lanosterol 14α-demethylase, causing ergosterol depletion and accumulation of C-14 methyl sterols, but they also have fungistatic activity against many fungi and are vulnerable to resistance. The echinocandins were introduced over a decade ago and inhibit synthesis of β-(1,3) glucan, a key component of the fungal cell wall, but they suffer from a restricted activity spectrum. Resistance to each class of antifungal has emerged, with infections becoming increasingly difficult to cure[3].

Combination therapy provides a promising strategy to enhance the efficacy of antifungals, impede drug resistance, and improve clinical outcome. Drug combinations are the standard of care for HIV, tuberculosis, and malaria, but have been less well explored for fungal infections[5]. There is great potential for targeting hubs in fungal cellular circuitry that are crucial for stress response, drug resistance, and virulence. The premier example is heat shock protein 90 (Hsp90), an essential molecular chaperone that stabilizes diverse cellular regulators[6]. Inhibition of Hsp90 abrogates drug resistance in diverse human fungal pathogens, rendering resistant infections responsive to treatment[7–9]. Hsp90 function can be modulated by natural products, such as geldanamycin and radicicol, as well as by diverse chemical scaffolds that have been developed to target Hsp90's key role in enabling malignant transformation[5]. Hsp90 regulates drug resistance by stabilizing the protein phosphatase calcineurin[9,10], which is the target of the natural products and immunosuppressants FK506 and cyclosporin A[11]. Although Hsp90 and calcineurin are promising antifungal drug targets, their therapeutic exploitation requires the development of fungal-selective

[1]Department of Molecular Genetics, University of Toronto, Toronto, Ontario, Canada. [2]Natural Products Center, School of Natural Resources and the Environment, College of Agriculture and Life Sciences, University of Arizona, Tucson, Arizona, USA. [3]Lunenfeld-Tanenbaum Research Institute, Mount Sinai Hospital, Toronto, Ontario, Canada. [4]Department of Molecular Genetics and Microbiology, Duke University Medical Center, Durham, North Carolina, USA. [5]Department of Biotechnology, College of Life Science and Biotechnology, Yonsei University, Seoul, Korea. [6]Department of Biotechnology and Biosciences, University of Milano-Bicocca and SYSBIO, Centre of Systems Biology, Milan, Italy. [7]Donnelly Centre for Cellular and Biomolecular Research, University of Toronto, Toronto, Ontario, Canada. [8]Institute of Biochemistry, Heinrich Heine University Duesseldorf, Duesseldorf, Germany. [9]Department of Molecular Biology, University of Geneva, Geneva, Switzerland. [10]Institute of Microbiology, University Hospital Lausanne and University Hospital Center, Lausanne, Switzerland. [11]Department of Medicine, University of Wisconsin, Madison, Wisconsin, USA. [12]Department of Medical Microbiology and Immunology, University of Wisconsin, Madison, Wisconsin, USA. [13]Faculty of Pharmaceutical Sciences, The University of British Columbia, Vancouver, British Columbia, Canada. *e-mail: leah.cowen@utoronto.ca

inhibitors to avoid host toxicity in the context of acute infections[5,11]. An alternative strategy is to identify new targets that are modulated by molecules that potentiate antifungal activity. The cyclic hexadepsipeptide natural product beauvericin (1) provides an ideal opportunity to identify targets for antifungal development, as it was found to be well tolerated by human cells and to be able to potentiate azole efficacy against *Candida parapsilosis* in a systemic infection model by a mechanism that remains enigmatic[12].

Here, we uncover dual activities of beauvericin and demonstrate its broad therapeutic potential. Beauvericin enhances azole efficacy against the leading human fungal pathogens, *Candida albicans*, *Aspergillus fumigatus*, and *Cryptococcus neoformans*, blocks the emergence of resistance, and renders resistant pathogens responsive to treatment. These effects are mediated via inhibition of multidrug efflux and TORC1 signaling, thereby activating protein kinase CK2 and inhibiting the molecular chaperone Hsp90. Substitutions in the efflux transporter Pdr5 that enable beauvericin efflux impair azole efflux, impeding resistance to the drug combination. Thus, dual targeting of multidrug efflux and TOR signaling provides a powerful and broadly effective therapeutic strategy for treating fungal infectious disease.

RESULTS

Beauvericin enhances azole efficacy and blocks resistance

We used antifungal test strips to produce a gradient of azole concentration in solid rich medium to test whether beauvericin enhances azole activity. Beauvericin had no antifungal activity alone, but enhanced azole efficacy against the model yeast *Saccharomyces cerevisiae* and fungal pathogens *C. albicans*, *C. neoformans*, and *A. fumigatus* (**Fig. 1a**). We used a dose–response matrix (checkerboard) to corroborate the synergy between the azole fluconazole and beauvericin against *C. albicans*, with a fractional inhibitory concentration index (FICI) of <0.1 (**Fig. 1b**). Transferring cells from the checkerboard onto drug-free rich medium revealed that beauvericin transforms azole fungistatic activity into a fungicidal combination (**Fig. 1b**).

Next, we compared the impact of beauvericin with that of geldanamycin (an Hsp90 inhibitor) and cyclosporin A (a calcineurin inhibitor) on azole resistance of *C. albicans* clinical isolates (CaCi) collected from an HIV-infected patient undergoing over 2 years of fluconazole treatment[9]. Beauvericin reduced resistance of all isolates (**Fig. 1c**), with cidality of the combination evident at higher azole concentrations (**Supplementary Results**, **Supplementary Fig. 1**).

Given the profound impact of beauvericin on azole resistance, we tested whether it blocks the emergence of resistance. We plated 1×10^5 *C. albicans* cells onto rich medium containing 32 μg/ml fluconazole, a high drug concentration that favors the rapid emergence of azole resistance[9]. Inclusion of beauvericin in the medium at a concentration that did not impair growth (20 μg/ml) blocked the emergence of resistance (**Fig. 1d**). Thus, beauvericin enhances azole efficacy against diverse fungal pathogens and blocks the emergence of azole resistance.

Pdr5 substitutions enable beauvericin efflux

A powerful strategy to identify drug targets and efflux mechanisms is to isolate and analyze drug-resistant mutants, as was accomplished for rapamycin with the discovery of FKBP12, Tor1, and Tor2 as its direct targets[13]. Given that beauvericin has little antifungal activity alone, we needed to define a sensitized background for selection experiments. We screened *S. cerevisiae* strains that each lacked one of 16 ATP-binding cassette (ABC) transporter genes[14], and found that only the strain lacking the ABC transporter *YOR1* was sensitive to beauvericin (**Supplementary Fig. 2**). This suggests that Yor1 effluxes beauvericin, and enables selection of resistant mutants.

To isolate beauvericin-resistant mutants in the *yor1*Δ background, we plated 1×10^8 cells onto rich medium with 100 μg/ml beauvericin and performed whole-genome sequencing of five

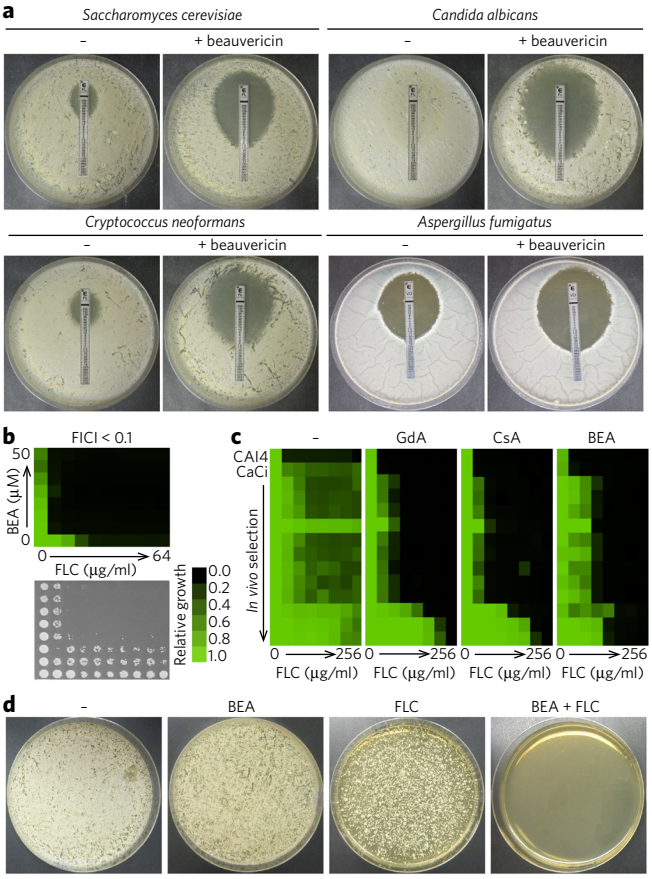

Figure 1 | Beauvericin enhances azole efficacy against diverse fungi and blocks the emergence of resistance. (**a**) Beauvericin reduces azole resistance in reference strains of *S. cerevisiae* (BY4741), *C. albicans* (SN95), and *C. neoformans* (H99a), and an *A. fumigatus* clinical isolate on rich YEPD medium. For the first three species, fluconazole strips generate a gradient from 0.016 to 256 μg/ml, with the highest concentration at the top. For *A. fumigatus*, voriconazole strips generate a gradient from 0.002–32 ng/ml. Where indicated, plates contained 20 μg/ml of beauvericin. Experiment was performed in biological triplicates. (**b**) Beauvericin (BEA) and fluconazole (FLC) are synergistic and cidal against *C. albicans* (SN95). SN95 was subjected to two-fold serial dilutions of BEA and FLC in YEPD at 30 °C for 48 h. Optical densities were standardized to drug-free controls (see "relative growth" bar) and FICI was calculated based on concentrations causing 60–70% growth inhibition. The drug combination is cidal, based on transferring cells to drug-free YEPD medium for 24 h. (**c**) BEA reduced FLC resistance of *C. albicans* clinical isolates (CaCi), similar to geldanamycin (GdA) and cyclosporin A (CsA). CaCi are ordered sequentially, with isolates recovered early at the top. CAI4 represents a fluconazole-sensitive laboratory strain of *C. albicans*. Minimum inhibitory concentration (MIC) assays were performed in YEPD (–) with GdA (5 μM), CsA (20 μM), or BEA (25 μM), with a two-fold serial dilution of FLC. Experiments in **b** and **c** were performed in biological triplicates with technical duplicates. (**d**) BEA blocks the emergence of FLC resistance in *C. albicans* (SN95). 1×10^5 cells were plated on YEPD containing no inhibitor (–), 20 μg/ml BEA, 32 μg/ml FLC, or the combination. Plates were photographed after 3 d at 30 °C. Experiment was performed in biological triplicates.

mutants. Each of the resistant mutants had at least one nonsynonymous mutation in the ABC transporter gene *PDR5* (**Fig. 2a**), which mapped to transmembrane domains or proximal regions. These are not loss-of-function mutations, as deletion of *PDR5* in the *yor1*Δ strain did not confer beauvericin resistance (**Fig. 2a**). We functionally validated that mutation in *PDR5* confers beauvericin resistance by focusing on $PDR5^{G538R}$, which corresponds to a residue that was mutated in three of the five mutants. Expression of $PDR5^{G538R}$ as the

© 2016 Nature America, Inc. All rights reserved.

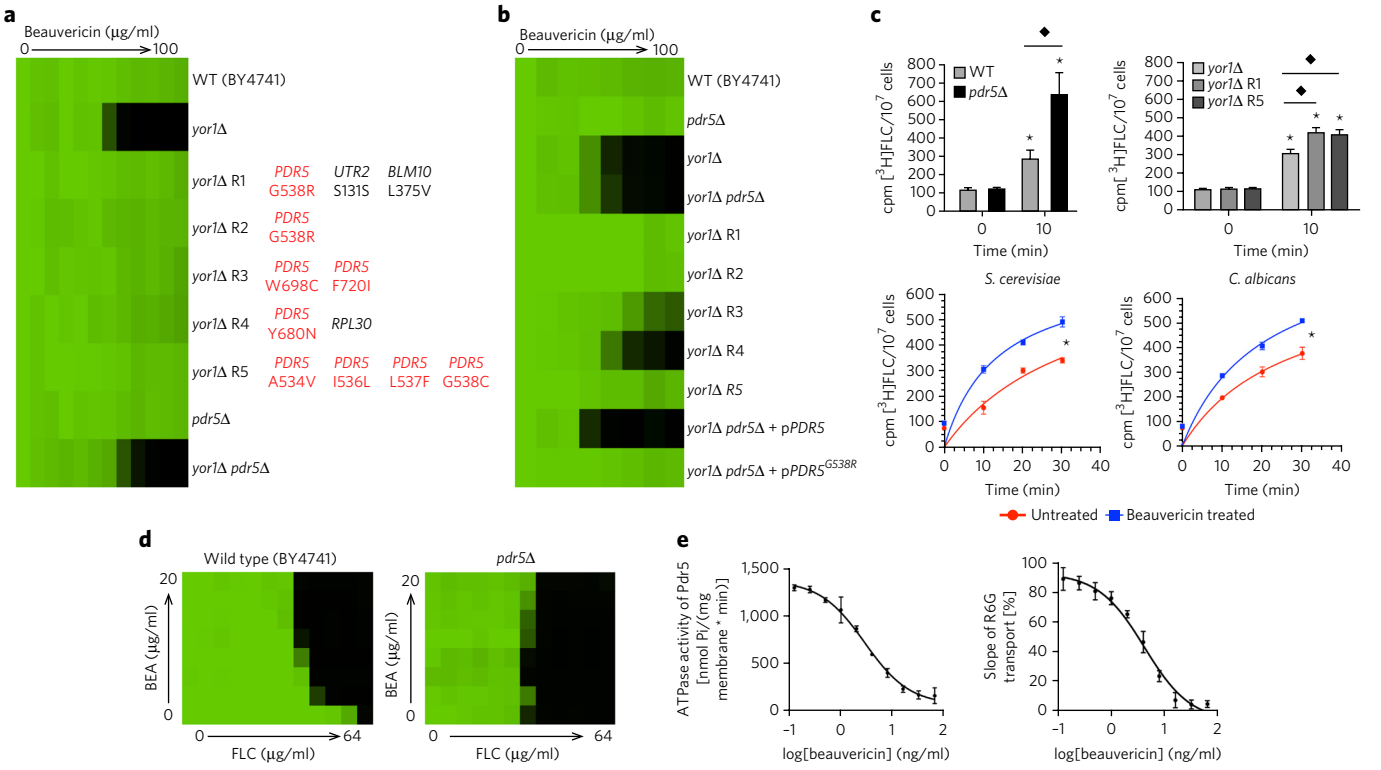

Figure 2 | Beauvericin inhibits Pdr5, thereby increasing fluconazole intracellular accumulation, and can be effluxed by Pdr5 following substitutions that alter substrate specificity. (**a**) *S. cerevisiae* lacking Yor1 is sensitive to beauvericin, but acquires resistance via Pdr5 substitutions. 1×10^8 cells were plated on YEPD containing beauvericin (100 μg/ml); resistant mutants were recovered after 3–4 d at 30 °C. Five beauvericin-resistant mutants, R1-R5, were selected for further characterization. Resistance was assessed in YEPD with two-fold serial dilutions of beauvericin, as in **Figure 1**. Mutations identified by genome sequencing are indicated as amino acid changes; mutations in *PDR5* are shown in red. (**b**) Functional validation of *PDR5* mutations. Amino acid 538 is altered in three of the five resistant mutants; expression of $PDR5^{G538R}$ in *yor1*Δ*pdr5*Δ confers beauvericin resistance. Resistance was assessed in synthetic defined (SD) medium at 30 °C for 72 h. Experiments in **a** and **b** were performed in biological triplicates with technical duplicates. (**c**) Beauvericin-resistant mutants exhibit altered substrate specificity, and beauvericin enhances azole accumulation. Top, intracellular accumulation of radiolabeled fluconazole ([^{3}H]FLC) in *pdr5*Δ as compared to wild-type (WT) *S. cerevisiae* and in the beauvericin-resistant mutants *yor1*Δ R1 and *yor1*Δ R5 as compared to *yor1*Δ. Error bars represent s.d., $*P < 0.05$ (paired *t*-test; 0 min versus 10 min), $\blacklozenge P < 0.05$ (unpaired *t*-test; WT 10 min versus *pdr5*Δ 10 min; *yor1*Δ 10 min versus *yor1*Δ R1 10 min and *yor1*Δ R5 10 min). Bottom, [^{3}H]FLC accumulation monitored in *S. cerevisiae* (BY4741) and *C. albicans* (SC5314) ± beauvericin (20 μg/ml). Error bars represent s.d., $*P < 0.05$ (paired *t*-test; untreated versus treated). (**d**) Synergy between beauvericin and fluconazole is blocked in *pdr5*Δ cells. Checkerboards as in **Figure 1b**; biological triplicates with technical duplicates. (**e**) Beauvericin inhibits Pdr5 ATPase activity and rhodamine-6G transport in *in vitro* plasma membrane assays. Error bars represent s.d. Experiments in **c** and **e** were performed in biological duplicates with technical replicates.

only *PDR5* allele in a *yor1*Δ mutant conferred full beauvericin resistance (**Fig. 2b**). Beauvericin is not a substrate of wild-type Pdr5, as deletion of *PDR5* did not enhance beauvericin susceptibility (**Fig. 2a**,**b**). Thus, these mutations may alter Pdr5 substrate specificity, enabling Pdr5-mediated beauvericin efflux.

Pdr5 transports a diverse set of structurally unrelated compounds, including azoles, cycloheximide, and rhodamines[15]. To determine if the *PDR5* mutations alter substrate specificity, we measured the accumulation of radiolabeled [^{3}H]fluconazole in the resistant mutants. Representative mutants *yor1*Δ R1 and *yor1*Δ R5 showed increased accumulation of radiolabeled azole (**Fig. 2c**, top panel). We also assessed the susceptibility of the resistant mutants to fluconazole, cycloheximide, and rhodamine-6G. Beauvericin-resistant mutants in the *yor1*Δ background all had increased susceptibility to the compounds, as did a *pdr5*Δ mutant (**Supplementary Fig. 3a–c**). The mutants also had increased accumulation of rhodamine-6G comparable to the *pdr5*Δ mutant (**Supplementary Fig. 4**). Together, these data suggest that Pdr5 substrate specificity is altered in the resistant mutants, enabling beauvericin efflux at the expense of other substrates. Thus, mutations in *PDR5* that enable beauvericin efflux impede azole efflux, thereby blocking the emergence of resistance to the drug combination.

Beauvericin enhances azole intracellular accumulation

To determine whether beauvericin itself might affect multidrug efflux, we monitored intracellular azole accumulation. Reduced azole accumulation is a prevalent mechanism of azole resistance, and inhibition of efflux transporters causes hypersusceptibility to azoles[2]. We found that beauvericin caused increased fluconazole accumulation in *S. cerevisiae* and *C. albicans* (**Fig. 2c**, bottom panel). Both the increase in fluconazole accumulation and the drug synergy were blocked in an *S. cerevisiae* strain lacking Pdr5 (**Fig. 2d** and **Supplementary Fig. 5**). To confirm that Pdr5 is a proximal target of beauvericin, we used *in vitro* plasma membrane assays of Pdr5 function[16]. Beauvericin inhibited Pdr5 ATPase activity and transport of rhodamine-6G (**Fig. 2e**). Thus, beauvericin enhances azole efficacy through inhibition of Pdr5, thereby causing increased azole accumulation within the fungal cell.

Mutations in CK2 subunits confer beauvericin resistance

Beauvericin must have an additional target beyond Pdr5 to mitigate antifungal activity in the absence of azoles, as Pdr5 is not required for viability of the wild type or *yor1*Δ mutant (**Fig. 2**). Furthermore, the fungistatic activity of azoles is independent of concentration (**Supplementary Fig. 1**), which suggests that the increase in

© 2016 Nature America, Inc. All rights reserved.

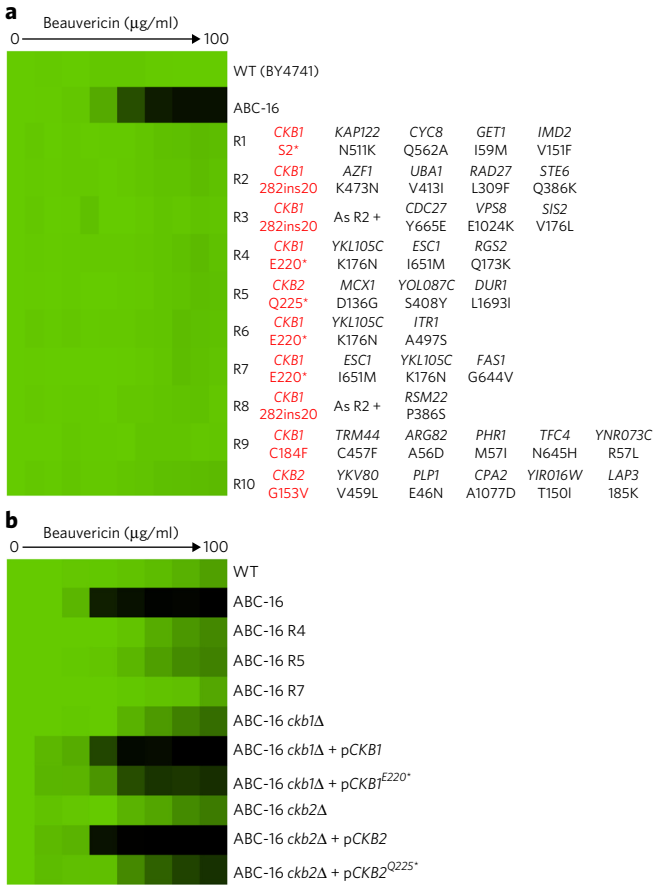

Figure 3 | Whole-genome sequencing of beauvericin-resistant mutants identifies mutations in protein kinase CK2. (**a**) The *S. cerevisiae* ABC16 strain, lacking 16 ABC transporters, is susceptible to beauvericin and was used to select for beauvericin-resistant mutants. Selection experiment was performed as in **Figure 2a**. Mutations identified by whole-genome sequencing of ten resistant mutants are indicated as amino acid changes. All resistant mutants had nonsynonymous mutations in genes encoding β-regulatory subunits of protein kinase CK2 (shown in red). Resistance phenotypes were assessed as in **Figure 2a**. (**b**) Loss of function of *CKB1* or *CKB2* confers beauvericin resistance in the ABC16 strain. Deletion of *CKB1* or *CKB2* in the ABC16 strain confers resistance to beauvericin. Expression of a wild-type allele of *CKB1* or *CKB2* in the ABC16 strain lacking the corresponding regulatory subunit gene restores beauvericin susceptibility to the level of the parental ABC16 strain; in contrast, resistance is maintained upon expression of the $CKB1^{E220*}$ or $CKB2^{Q225*}$ alleles. Resistance phenotypes were assessed as in **Figure 2b**. Experiments in **a** and **b** were performed in biological triplicates with technical duplicates.

intracellular azole accumulation upon beauvericin-mediated inhibition of efflux does not confer the fungicidal activity. To enhance our capacity to identify beauvericin targets and minimize effects of efflux, we selected for beauvericin-resistant mutants in an *S. cerevisiae* strain lacking all 16 ABC transporters within clades implicated in multidrug resistance (ABC16) (ref. 14). We plated 1×10^8 cells onto rich medium containing 100 μg/ml beauvericin. Whole-genome sequencing of ten resistant mutants revealed that each harbored a mutation in either *CKB1* or *CKB2*, encompassing six independent mutational events (**Fig. 3a**). *CKB1* and *CKB2* encode the non-redundant β-regulatory subunits of protein kinase CK2, which is an essential serine and threonine protein kinase that phosphorylates over 300 substrates, including Hsp90 (ref. 17). The *S. cerevisiae* CK2 complex is composed of two α-catalytic subunits (α and α′, encoded by *CKA1* and *CKA2*, respectively) and two β-regulatory subunits (β and β′) that can exist as free α-catalytic subunits or as an $\alpha_2\beta_2$ holoenzyme, with different substrate specificity[18]. Deletion of either *CKB1* or *CKB2* in the ABC16 background conferred full beauvericin resistance, suggesting that the mutations identified cause loss of function of CK2 subunits (**Fig. 3b**). Consistent with this model, expression of wild-type *CKB1* in the ABC16 *ckb1*Δ strain restored beauvericin susceptibility, while expression of $CKB1^{E220*}$ maintained resistance (**Fig. 3b**). Comparable results were obtained with the ABC16 *ckb2*Δ strain upon expression of wild-type *CKB2* or mutant $CKB2^{Q225*}$ (**Fig. 3b**). Although mutations in genes encoding the catalytic subunits were not identified, we found that deletion of either *CKA1* or *CKA2* from the ABC16 strain confers partial resistance to beauvericin (**Supplementary Fig. 6**); the smaller impact on resistance likely explains why mutations in these genes were not identified in our selection experiment. Thus, loss of function of CK2 subunits confers beauvericin resistance, suggesting that beauvericin exerts antifungal activity via CK2.

Biotinylated beauvericin interacts with Cka2 and Tor2

Next, we took a complementary proteomic approach to identify beauvericin targets. We synthesized a biotinylated beauvericin analog, biotinyloxybeauvericin (**2**) (**Fig. 4a** and **Supplementary Note 1**), which retains antifungal activity (**Supplementary Fig. 7**), and performed affinity purification coupled to mass spectrometry (AP–MS) with a wild-type *S. cerevisiae* strain. AP–MS was performed under three distinct buffer conditions with biological duplicates and negative controls. To identify significant interactions, results for biotinylated beauvericin were compared to those for beads-only controls and were subjected to statistical analysis using SAINTexpress[19]. Proteins with false discovery rates equal or below 1% were classified as statistically significant beauvericin targets. Twelve proteins were identified in at least two of the three experiments (**Fig. 4a**). Two experiments identified Cka2 as a top interacting protein, thereby corroborating the link between beauvericin and CK2. Other components of the CK2 complex were not identified, which suggests that Cka2 may be the proximal target and that the complex was not preserved during affinity purification. Excess unmodified beauvericin did not compete the biotinylated analog from most proteins, including Cka2, likely as a result of the very high local concentration of the biotinylated analog at bound targets. Consistent with this idea, we observed competitive displacement of another top interacting protein with functional connections to CK2, Tor2, only with the highest concentration of unmodified beauvericin tested (**Fig. 4a**). Tor2 was identified in all three experiments and is a component of the target of rapamycin complex 1 and 2 (TORC1 and TORC2) (ref. 20); TORC1 regulates phosphorylation of CK2 via the effector kinase Kns1 (ref. 21). Thus, CK2 and TOR may be the binding targets of beauvericin, through which it exerts antifungal activity.

Beauvericin activates CK2 and inhibits TORC1

Given that beauvericin binds to a catalytic subunit of protein kinase CK2 and that the loss of function of CK2 subunits confers beauvericin resistance, we assessed whether beauvericin modulates CK2 activity. We monitored phosphorylation of Sic1, a cyclin-dependent kinase inhibitor that is phosphorylated by the CK2 holoenzyme at serine 201 (refs. 22,23). ABC16 cells or lysates were incubated with beauvericin or vehicle and the subsequent CK2 activity was monitored by quantifying Sic1 phosphorylation in an *in vitro* assay. Beauvericin increased Sic1 phosphorylation, suggesting that it activates CK2 (**Fig. 4b** and **Supplementary Fig. 8a**). As expected, there was no detectable CK2 holoenzyme activity in the beauvericin-resistant CK2 mutants (**Supplementary Fig. 8b**). To determine if this effect is direct, we monitored Sic1 phosphorylation using an *in vitro* kinase-activity assay with recombinant human CK2 subunits. Addition of either CK2α or $CK2\alpha_2\beta_2$ caused increased Sic1 phosphorylation that was not altered by beauvericin (**Supplementary**

© 2016 Nature America, Inc. All rights reserved.

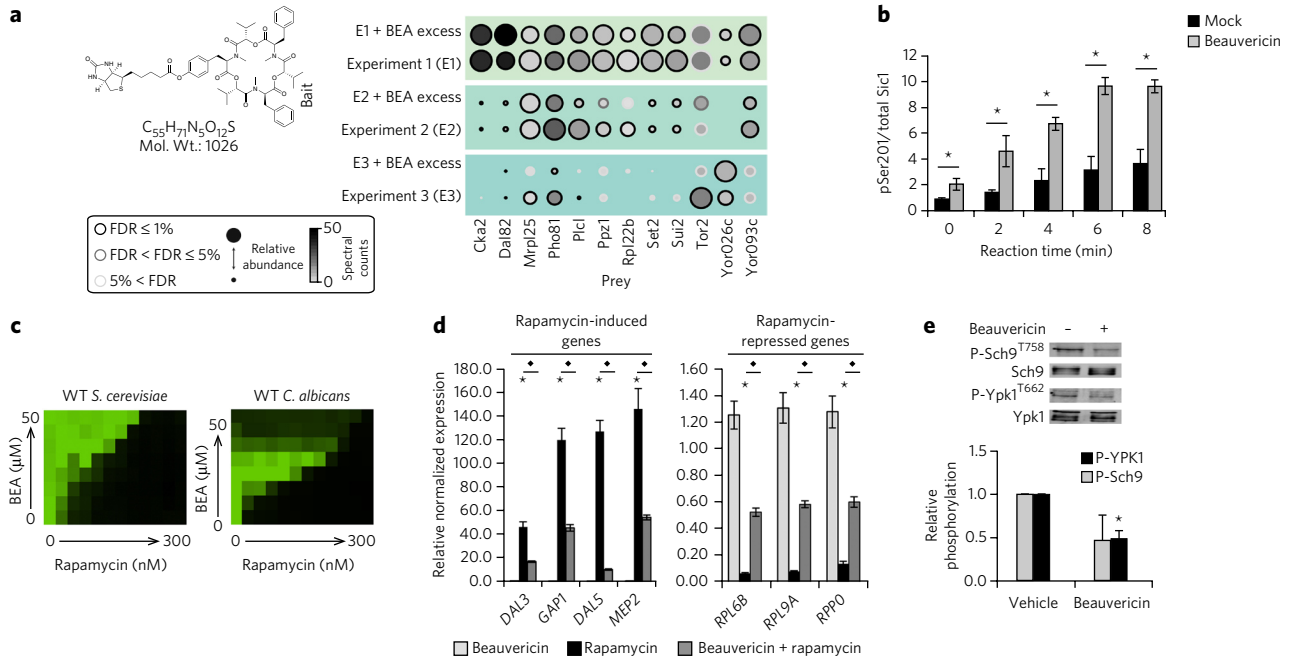

Figure 4 | Beauvericin binds to protein kinases Tor2 and CK2 and modulates their activity. (**a**) Left, structure of the beauvericin (BEA) biotinylated analog. Right, AP–MS with three buffer conditions in biological duplicates. Circle color indicates absolute spectral count, size indicates relative protein abundance, and edge indicates SAINT false discovery rate (FDR). Excess unmodified beauvericin added as competitor (E1: 2× excess, E2: 14× excess, and E3: 25× excess). (**b**) Beauvericin enhances CK2 activity. Phosphorylation of CK2 targets Sic1 monitored in an *in vitro* assay using protein lysates from the ABC16 strain, adding beauvericin or vehicle (Mock) to the reaction. Assay in biological duplicates with technical replicates. Error bars represent s.d.; $^*P < 0.05$ (*t*-test). (**c**) Beauvericin and rapamycin are antagonistic. Beauvericin suppresses rapamycin antifungal activity against *S. cerevisiae* (BY4741) and *C. albicans* (SN95). Checkerboards were performed as in **Figure 1b**, but for 24 h. Checkerboards performed in biological triplicates with technical duplicates. (**d**) Beauvericin reduces gene induction and repression in response to rapamycin in *S. cerevisiae*. Transcript levels of treated (0.2 μg/ml rapamycin; 40 μg/ml beauvericin) and untreated cells measured by qRT-PCR and normalized to *ACT1* and untreated sample. Error bars represent s.d. among technical triplicates. Assay is representative of biological triplicates. $^*P < 0.05$ compared to untreated, $^♦P < 0.05$ compared to rapamycin treatment (ANOVA). (**e**) Beauvericin inhibits TORC1 activity. Phosphorylation of TORC1 target (Sch9) and TORC2 target (Ypk1) monitored in *yor1*Δ grown ± 5 μg/ml beauvericin for 4 h before protein extraction and western blot analysis. P, phosphorylation. Error bars represent s.d. among biological triplicate experiments. $^*P < 0.05$ compared to vehicle (unpaired *t*-test).

© 2016 Nature America, Inc. All rights reserved.

Fig. 8c). This suggests that either beauvericin does not directly affect CK2 activity, or that the effects are specific to fungal CK2.

Next, we explored whether beauvericin modulates CK2 function indirectly through effects on TORC1. The TORC1 complex, composed of either Tor1 or Tor2, as well as Kog1, Lst8 and Tco89, is a global sensor of nutrient availability and regulates diverse cellular processes including growth, protein synthesis, cell cycle, and transcription[20,24]. TORC1 function is modulated by rapamycin, which binds to the FKBP12 proline rotamase to form a protein–drug complex that binds to TOR proteins and inhibits TORC1 function[13]. If beauvericin modulates TORC1 activity by binding to Tor2, then we would expect an interaction between beauvericin and rapamycin. To test this, we performed checkerboard assays with a gradient of rapamycin and beauvericin against *S. cerevisiae* and *C. albicans*. We observed potent antagonism, such that beauvericin suppressed the antifungal activity of rapamycin (**Fig. 4c**). The interaction between beauvericin and rapamycin was abrogated by deletion of genes encoding FKBP12 (*FPR1* in *S. cerevisiae, RBP1* in *C. albicans*)[25] and was impervious to deletion of *PDR5* (**Supplementary Fig. 9**), confirming that the effects are mediated via TOR. To corroborate the antagonism between beauvericin and rapamycin, we used quantitative RT-PCR to monitor transcript levels of genes whose expression is modulated by rapamycin-dependent inhibition of TOR function[26]. Beauvericin alone had no impact on transcript levels, but it partially blocked induction of four TOR-dependent permease or hydrolase genes and repression of three TOR-dependent ribosomal genes in response to rapamycin (**Fig. 4d**). This suggests that beauvericin may bind to Tor2 in a manner that antagonizes the interaction between the rapamycin–FKBP12 complex and TORC1.

To more directly evaluate whether beauvericin modulates TOR function, we monitored phosphorylation of two TOR-dependent substrates, Sch9 (TORC1) and Ypk1 (TORC2). Beauvericin caused a significant reduction in Sch9 phosphorylation and a modest reduction in Ypk1 phosphorylation (**Fig. 4e** and **Supplementary Fig. 10**). Together, these results suggest that beauvericin activates CK2 by binding to Tor2 and inhibiting TORC1 function.

Beauvericin impairs Hsp90 function

One key target of CK2 is the molecular chaperone Hsp90, a global regulator of antifungal drug resistance. Hsp90 regulates cellular responses required to survive drug-induced stress, and inhibition of Hsp90 transforms azoles from fungistatic to fungicidal[7,9]. In *S. cerevisiae* and *C. albicans*, CK2 phosphorylates Hsp90, thereby modulating chaperone function[27,28]. To determine whether the effects of beauvericin on TORC1 and CK2 impair Hsp90 function, we monitored the activity of the Hsp90 client proteins calcineurin[10], heat shock transcription factor Hsf1 (ref. 29), and mitogen-activated protein kinase Hog1 (refs. 28,30). Calcineurin is a protein phosphatase that, when activated, dephosphorylates the transcription factor Crz1, which in turn enables Crz1 nuclear localization and binding to calcineurin-dependent response elements (CDREs) in target gene promoters, thereby driving gene expression[31]. To determine if beauvericin impairs calcineurin function, we used an *S. cerevisiae* strain harboring a reporter in which CDREs drive *lacZ*

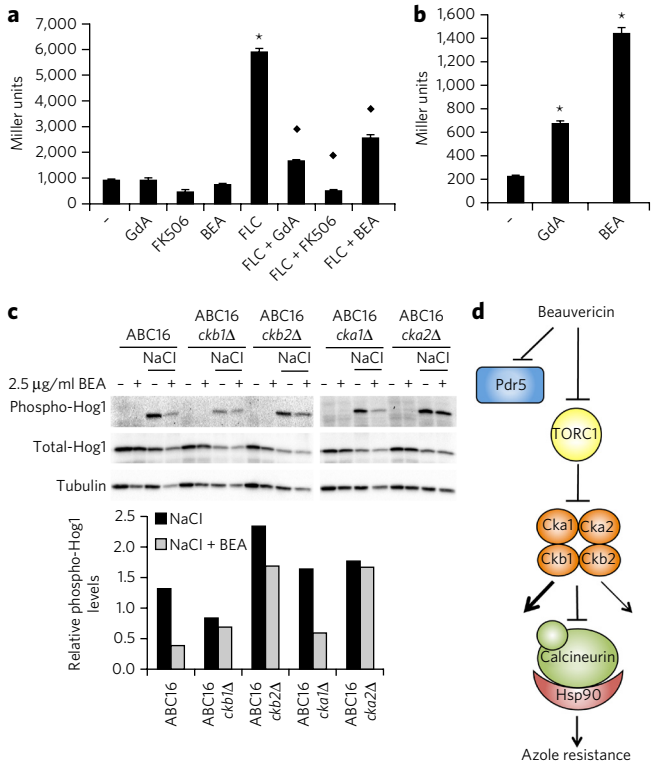

Figure 5 | Beauvericin inhibits Hsp90 function. (**a**) Beauvericin (BEA) reduces fluconazole-induced calcineurin activation. Shown is a quantification of calcineurin activation as measured using a strain of *S. cerevisiae* harboring a 4xCDRE-*lacZ* reporter construct with or without treatment with fluconazole (FLC, 64 μg/ml) and/or either geldanamycin (GdA, 5.6 μg/ml), FK506 (1.0 μg/ml) or beauvericin (20 μg/ml). Miller units represent quantification of β-galactosidase activity through the production of *lacZ*. Data are mean ± s.d. from technical triplicates and representative of biological replicates. *$P < 0.05$ relative to untreated, ♦$P < 0.05$ relative to fluconazole treatment (ANOVA, Tukey *post hoc* test). (**b**) Beauvericin induces the heat shock response. *C. albicans* containing *HSP70p-lacZ* reporter construct were untreated (−) or treated with geldanamycin (10 μM) or beauvericin (13 μM); both induced expression from the *HSP70* promoter. Data representation as described in **a**. *$P < 0.05$. (**c**) Beauvericin blocks Hog1 activation in a manner that depends on CK2 subunits. Sodium chloride (NaCl) was used to activate Hog1. Beauvericin (2.5 μg/ml) reduced levels of phosphorylated Hog1 in the ABC16 strain; deletion of *CKB1* or *CKA2* reduced the effect of beauvericin. Bands were quantified using ImageJ, and the ratio of phosphorylated Hog1 to total Hog1 plotted for one biological replicate. Tubulin was used as a loading control. A similar trend was observed in biological triplicate experiments (**Supplementary Fig. 12**). (**d**) Model for beauvericin mechanism of action. Beauvericin inhibits Pdr5, thereby enabling increased azole intracellular accumulation. Beauvericin also inhibits TORC1, thereby activating CK2. Increased CK2 activity has pleiotropic effects including inhibiting the function of Hsp90 and its client protein calcineurin, which regulate azole resistance.

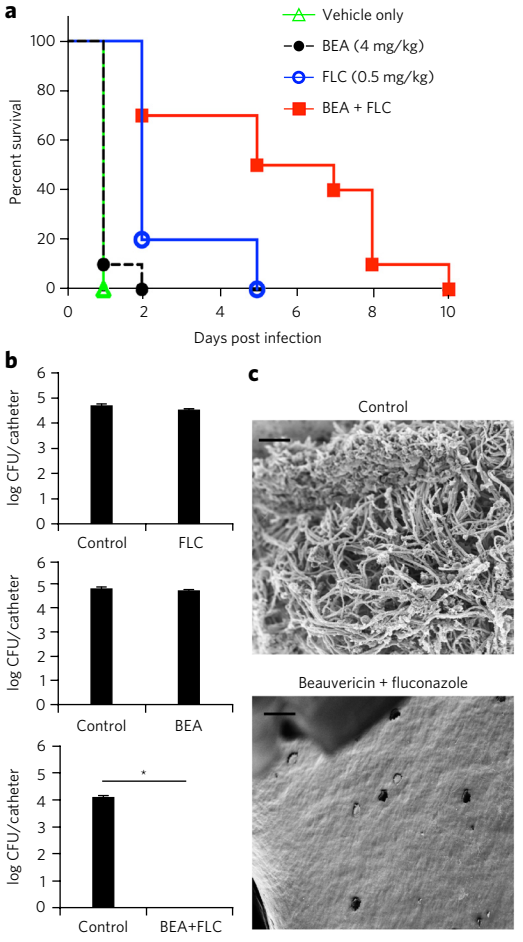

Figure 6 | The combination of beauvericin and fluconazole provides a powerful therapeutic strategy. (**a**) Beauvericin (BEA) enhances fluconazole (FLC) efficacy in a mouse model of *C. albicans* disseminated infection. Mice were infected with *C. albicans* (SC5314) and treated with vehicle, beauvericin, fluconazole, or the combination. Even with a high *C. albicans* inoculum, the combination of beauvericin and fluconazole significantly enhanced survival relative to either treatment alone. Each group consisted of 10 female BALB/c mice. Log-rank (Mantel-Cox) test vehicle versus beauvericin: $P = 0.3173$, vehicle versus fluconazole: $P < 0.0001$, vehicle versus combination: $P < 0.0001$, beauvericin versus combination: $P < 0.0001$, and fluconazole versus combination: $P = 0.0061$. (**b**) The combination of beauvericin (4 μg/ml) and fluconazole (500 μg/ml) eradicates *C. albicans* biofilm infections in a rat central venous catheter model. 1×10^6 cells of wild-type *C. albicans* (SC5314) were inoculated in rat venous catheters for 24 h followed by intraluminal drug treatment for 24 h. Catheters were surgically removed, and serial dilutions of the catheter fluid were plated for viable fungal colony counts in triplicate. Data represented as mean colony forming units (CFU) per catheter ± s.d.; one 12-week-old female (Sprague-Dawley) rat per treatment. The combination of fluconazole and beauvericin reduces fungal burden in the catheter compared to individual drug treatments (*$P < 0.05$, unpaired *t*-test). (**c**) Scanning electron microscopy (SEM) images of biofilms formed on rat catheters highlight the efficacy of the combination treatment, which sterilizes the catheter. Biofilms were processed as described in **b**, and catheters were visualized by s.e.m. All images are at 1,000× magnification (scale bars 20 μM).

expression[31]. Activation of calcineurin in response to fluconazole was blocked by the calcineurin inhibitor FK506 and was partially blocked by the Hsp90 inhibitor geldanamycin and by beauvericin (**Fig. 5a**).

To corroborate the effects of beauvericin on Hsp90 function, we monitored induction of the heat shock response (HSR) in *C. albicans*. Hsp90 exerts a repressive effect on Hsf1 that is relieved when Hsp90 function is compromised[6]. Upon activation, Hsf1 binds to heat shock elements (HSEs) in promoters of HSR genes, such as *HSP70*. To monitor activation of the HSR, we used a reporter in which the promoter of *HSP70* is fused to *lacZ* and integrated at the native *HSP70* locus[32]. As expected, inhibition of Hsp90 with geldanamycin induced expression from the *HSP70* promoter, indicative of HSR activation (**Fig. 5b**). Beauvericin potently induced the HSR (**Fig. 5b**), consistent with a repressive effect on Hsp90 function.

© 2016 Nature America, Inc. All rights reserved.

Lastly, we further validated the effects of beauvericin on Hsp90 function by monitoring Hog1 activation, and determined whether the effects were mediated via CK2. Hog1 requires Hsp90 to enable its activation by phosphorylation[28,30]. We tested whether beauvericin reduces Hog1 activation in response to osmotic stress induced by sodium chloride in the *S. cerevisiae* ABC16 strain and derivatives lacking CK2 subunits. Consistent with a repressive effect on Hsp90, beauvericin impaired Hog1 activation in the ABC16 strain (**Fig. 5c** and **Supplementary Fig. 11**). This effect is likely carried out through CK2, given that deletion of *CKB1* or *CKA2* reduced the impact of beauvericin on Hog1 activation (**Fig. 5c**). Deletion of *CKB2* or *CKA1* had only a minor impact, suggesting functional differentiation among CK2 subunits. Levels of phosphorylated Hog1 were normalized to total Hog1 (**Fig. 5c**), and the findings were confirmed with biological triplicate experiments (**Supplementary Fig. 12**). Thus, beauvericin exerts a repressive effect on Hsp90 via activation of CK2 signaling, providing a mechanism by which beauvericin abrogates azole resistance and creates a fungicidal drug combination (**Fig. 5d**).

Beauvericin potentiates azole therapeutic efficacy

The potent synergy of beauvericin with azoles suggests that it may have potential for use as a therapeutic in combination therapy. To test this, we first used a well-established murine model of *C. albicans* disseminated infection. Mice were infected with 5×10^6 *C. albicans* cells and treated daily with vehicle, beauvericin (4 mg/kg), fluconazole (0.5 mg/kg), or the combination. In the absence of treatment, mice succumbed to the infection within 2 days, demanding rapid therapeutic effects. As single agents, beauvericin had no impact, while fluconazole had a minor benefit (**Fig. 6a**). As a combination, there was potent therapeutic benefit of beauvericin and fluconazole (**Fig. 6a**).

Next, we evaluated the therapeutic potential of the beauvericin and fluconazole drug combination against *C. albicans* biofilms. *C. albicans* biofilms are complex communities that form on tissues and implanted medical devices; they are inherently drug resistant, such that surgical removal of infected devices is often required to eradicate infections[2]. We used a rat central-venous catheter model of *C. albicans* biofilm infection to assess possible drug combination therapy[8]. As single agents, treatment with either fluconazole or beauvericin had no therapeutic benefit (**Fig. 6b**). As a drug combination, beauvericin and fluconazole sterilized the catheter (**Fig. 6b**,**c**). Thus, beauvericin has profound therapeutic benefits in combination with azoles in mammalian infection models.

DISCUSSION

Our findings revealed that dual targeting of multidrug efflux and TOR signaling provides a powerful strategy to enhance antifungal efficacy, impede drug resistance, and render resistant pathogens responsive to treatment. We established that the natural product beauvericin inhibits multidrug efflux, thereby enhancing azole intracellular accumulation and potentiating azole antifungal activity. Beauvericin also inhibits TOR signaling, thereby stimulating protein kinase CK2 and inhibiting Hsp90. Hsp90 potentiates azole resistance by enabling crucial cellular responses to drug-induced stress that are independent from multidrug efflux[9], suggesting that beauvericin simultaneously undermines two core resistance mechanisms. This work illuminates the molecular mechanism of antifungal synergy between beauvericin and azoles that has remained enigmatic for decades[12,33], and highlights a new therapeutic strategy to treat life-threatening fungal infectious disease.

Linking bioactive molecules to their cellular targets is a major challenge that is crucial for the development of chemical probes for biomedical research and for discovery of new therapeutics[34]. We harnessed genome sequencing and affinity purification of a biotinylated beauvericin analog to identify the target and mechanism of action. In a transporter-deficient background, genome sequencing and functional analysis of beauvericin-resistant mutants identified loss of function of CK2 regulatory subunits as a resistance mechanism. Affinity purification of a biotinylated analog revealed an interaction with a catalytic subunit of protein kinase CK2 (Cka2) and protein kinase Tor2, which participates in TORC1 and TORC2 complexes that regulate diverse cellular processes, including substrate specificity of CK2 (refs. 21,35). The discovery that beauvericin inhibits TORC1 and suppresses the antifungal activity of the TORC1 inhibitor rapamycin suggests that beauvericin may lock TOR in a conformation that the rapamycin–FKBP12 complex is unable to bind to. Deletion of *CKA2* increases azole resistance[36], which is consistent with our findings that activation of CK2 abrogates resistance. Although CK2 is a constitutively active, promiscuous kinase with over 300 targets, its substrate specificity is modulated by phosphorylation[21], causing increased phosphorylation of specific targets. It is likely that the beauvericin-resistant mutants acquired mutations in CK2 genes rather than in *TOR2*, given that *TOR2* is essential. Ultimately, beauvericin causes inhibition of Hsp90 function based on analysis of three clients; the heat shock transcription factor Hsf1, the protein phosphatase calcineurin, and the protein kinase Hog1. CK2 phosphorylates Hsp90, and perturbation of CK2 modulates Hsp90 chaperone function[27,28]. Thus, we establish a novel mechanism to modulate signaling through global cellular regulators TOR, CK2, and Hsp90.

The capacity of beauvericin to simultaneously modulate core cellular signaling and inhibit multidrug efflux overcomes a major challenge for small molecule efficacy against fungi, which are the elaborate efflux systems that confer resistance to a multitude of drugs. This is reminiscent of the natural products FK506 and cyclosporin A, which exert potent inhibitory effects on both the protein phosphatase calcineurin and multidrug efflux[37,38]. Beauvericin inhibits multidrug efflux, thereby causing increased intracellular accumulation of azoles and potentiating azole antifungal activity. Despite the potent synergy of beauvericin with azoles, it has little antifungal activity alone due to efflux mediated by the ABC transporter Yor1, which is the homolog of the human cystic fibrosis transmembrane receptor (CFTR)[39]. Importantly, this efflux does not impair the capacity of beauvericin to abrogate azole resistance and enhance the efficacy of azoles in mammalian infection models. That beauvericin activates the heat shock response in cells with intact efflux systems suggests that there is sufficient intracellular accumulation to modulate cellular signaling. Strikingly, substitutions in the ABC transporter Pdr5 that alter substrate specificity and enable beauvericin efflux concomitantly impair azole efflux, thereby impeding the emergence of resistance to the drug combination.

Natural products have provided an unparalleled source of therapeutic agents that have revolutionized modern medicine, with beauvericin expanding the repertoire that modulates key eukaryotic regulators. The vast majority of antibacterials are naturally derived, as are two of the three major classes of antifungals (polyenes and echinocandins)[40]. Microbial natural products also provide some of the most promising leads for abrogating antifungal drug resistance by crippling stress response pathways. For example, bacterial and fungal species produce diverse chemical scaffolds that inhibit Hsp90 (ref. 41). For soil-dwelling bacteria such as the *Streptomycetes* that produce Hsp90 inhibitors, this may provide them with an advantage in microbial communities by inhibiting the growth of fungal competitors. Hsp90 inhibitors are also produced by diverse fungi, including mycopathogens, plant pathogens, and plant symbiotes[41]. For fungi, production of Hsp90 inhibitors to which they are resistant may be key for the establishment of parasitic or symbiotic relationships. Bacteria that produce the calcineurin inhibitor FK506 or the TOR inhibitor rapamycin and the fungi that produce the calcineurin inhibitor cyclosporin A may reap similar rewards. Beauvericin is produced by diverse fungi, including *Fusarium*

© 2016 Nature America, Inc. All rights reserved.

species and the entomopathogen *Beauveria bassiana*, for which the production of beauvericin enables virulence in insect hosts[42]. This illustrates a stunning convergence of natural products on interconnected hubs of eukaryotic cellular signaling, with profound implications for organismal interactions in nature.

Targeting cellular regulators of stress response and drug resistance has broad therapeutic relevance. Combined inhibition of stress response regulators and antimicrobial drug targets can improve therapeutic outcomes by enabling reduced doses of individual agents, more effectively eradicating pathogen populations, and impeding the emergence of drug resistance[9,43]. Beyond fungal pathogens, inhibitors of Hsp90, calcineurin, and TOR have potent activity against protozoan parasites, including those causing malaria, trypanosomiasis, and toxoplasmosis[5,44,45]. Beauvericin also has a remarkable breadth of activity with antibiotic, antifungal, insecticidal, and anticancer activity[46]. There is phenomenal potential in exploiting the utility of molecules that have been optimized as antimicrobials over the course of evolution.

Received 20 November 2015; accepted 3 June 2016;
published online 29 August 2016

METHODS

Methods and any associated references are available in the online version of the paper.

References

1. Brown, G.D. *et al.* Hidden killers: human fungal infections. *Sci. Transl. Med.* **4**, 165rv13 (2012).
2. Shapiro, R.S., Robbins, N. & Cowen, L.E. Regulatory circuitry governing fungal development, drug resistance, and disease. *Microbiol. Mol. Biol. Rev.* **75**, 213–267 (2011).
3. Denning, D.W. & Bromley, M.J. Infectious disease. How to bolster the antifungal pipeline. *Science* **347**, 1414–1416 (2015).
4. Anderson, T.M. *et al.* Amphotericin forms an extramembranous and fungicidal sterol sponge. *Nat. Chem. Biol.* **10**, 400–406 (2014).
5. Cowen, L.E. The fungal Achilles' heel: targeting Hsp90 to cripple fungal pathogens. *Curr. Opin. Microbiol.* **16**, 377–384 (2013).
6. Leach, M.D., Klipp, E., Cowen, L.E. & Brown, A.J.P. Fungal Hsp90: a biological transistor that tunes cellular outputs to thermal inputs. *Nat. Rev. Microbiol.* **10**, 693–704 (2012).
7. Cowen, L.E. *et al.* Harnessing Hsp90 function as a powerful, broadly effective therapeutic strategy for fungal infectious disease. *Proc. Natl. Acad. Sci. USA* **106**, 2818–2823 (2009).
8. Robbins, N. *et al.* Hsp90 governs dispersion and drug resistance of fungal biofilms. *PLoS Pathog.* **7**, e1002257 (2011).
9. Cowen, L.E. & Lindquist, S. Hsp90 potentiates the rapid evolution of new traits: drug resistance in diverse fungi. *Science* **309**, 2185–2189 (2005).
10. Singh, S.D. *et al.* Hsp90 governs echinocandin resistance in the pathogenic yeast *Candida albicans* via calcineurin. *PLoS Pathog.* **5**, e1000532 (2009).
11. Steinbach, W.J., Reedy, J.L., Cramer, R.A. Jr., Perfect, J.R. & Heitman, J. Harnessing calcineurin as a novel anti-infective agent against invasive fungal infections. *Nat. Rev. Microbiol.* **5**, 418–430 (2007).
12. Zhang, L. *et al.* High-throughput synergy screening identifies microbial metabolites as combination agents for the treatment of fungal infections. *Proc. Natl. Acad. Sci. USA* **104**, 4606–4611 (2007).
13. Heitman, J., Movva, N.R. & Hall, M.N. Targets for cell cycle arrest by the immunosuppressant rapamycin in yeast. *Science* **253**, 905–909 (1991).
14. Suzuki, Y. *et al.* Knocking out multigene redundancies via cycles of sexual assortment and fluorescence selection. *Nat. Methods* **8**, 159–164 (2011).
15. Prasad, R. & Goffeau, A. Yeast ATP-binding cassette transporters conferring multidrug resistance. *Annu. Rev. Microbiol.* **66**, 39–63 (2012).
16. Gupta, R.P., Kueppers, P., Hanekop, N. & Schmitt, L. Generating symmetry in the asymmetric ATP-binding cassette (ABC) transporter Pdr5 from *Saccharomyces cerevisiae*. *J. Biol. Chem.* **289**, 15272–15279 (2014).
17. Miyata, Y. Protein kinase CK2 in health and disease: CK2: the kinase controlling the Hsp90 chaperone machinery. *Cell. Mol. Life Sci.* **66**, 1840–1849 (2009).
18. Kubiński, K. *et al.* Yeast holoenzyme of protein kinase CK2 requires both beta and beta' regulatory subunits for its activity. *Mol. Cell. Biochem.* **295**, 229–236 (2007).
19. Teo, G. *et al.* SAINTexpress: improvements and additional features in Significance Analysis of INTeractome software. *J. Proteomics* **100**, 37–43 (2014).
20. Martin, D.E. & Hall, M.N. The expanding TOR signaling network. *Curr. Opin. Cell Biol.* **17**, 158–166 (2005).
21. Sanchez-Casalongue, M.E. *et al.* Differential phosphorylation of a regulatory subunit of protein kinase CK2 by target of rapamycin complex 1 signaling and the Cdc-like kinase Kns1. *J. Biol. Chem.* **290**, 7221–7233 (2015).
22. Coccetti, P. *et al.* Mutations of the CK2 phosphorylation site of Sic1 affect cell size and S-Cdk kinase activity in *Saccharomyces cerevisiae*. *Mol. Microbiol.* **51**, 447–460 (2004).
23. Coccetti, P. *et al.* Sic1 is phosphorylated by CK2 on Ser201 in budding yeast cells. *Biochem. Biophys. Res. Commun.* **346**, 786–793 (2006).
24. Loewith, R. *et al.* Two TOR complexes, only one of which is rapamycin sensitive, have distinct roles in cell growth control. *Mol. Cell* **10**, 457–468 (2002).
25. Cruz, M.C. *et al.* Rapamycin and less immunosuppressive analogs are toxic to *Candida albicans* and *Cryptococcus neoformans* via FKBP12-dependent inhibition of TOR. *Antimicrob. Agents Chemother.* **45**, 3162–3170 (2001).
26. Cardenas, M.E., Cutler, N.S., Lorenz, M.C., Di Como, C.J. & Heitman, J. The TOR signaling cascade regulates gene expression in response to nutrients. *Genes Dev.* **13**, 3271–3279 (1999).
27. Mollapour, M. *et al.* Threonine 22 phosphorylation attenuates Hsp90 interaction with cochaperones and affects its chaperone activity. *Mol. Cell* **41**, 672–681 (2011).
28. Diezmann, S., Michaut, M., Shapiro, R.S., Bader, G.D. & Cowen, L.E. Mapping the Hsp90 genetic interaction network in *Candida albicans* reveals environmental contingency and rewired circuitry. *PLoS Genet.* **8**, e1002562 (2012).
29. Leach, M.D. *et al.* Hsp90 orchestrates transcriptional regulation by Hsf1 and cell wall remodelling by MAPK signalling during thermal adaptation in a pathogenic yeast. *PLoS Pathog.* **8**, e1003069 (2012).
30. Hawle, P. *et al.* Cdc37p is required for stress-induced high-osmolarity glycerol and protein kinase C mitogen-activated protein kinase pathway functionality by interaction with Hog1p and Slt2p (Mpk1p). *Eukaryot. Cell* **6**, 521–532 (2007).
31. Stathopoulos, A.M. & Cyert, M.S. Calcineurin acts through the CRZ1/TCN1-encoded transcription factor to regulate gene expression in yeast. *Genes Dev.* **11**, 3432–3444 (1997).
32. Shapiro, R.S. *et al.* Hsp90 orchestrates temperature-dependent *Candida albicans* morphogenesis via Ras1-PKA signaling. *Curr. Biol.* **19**, 621–629 (2009).
33. Fukuda, T., Arai, M., Tomoda, H. & Omura, S. New beauvericins, potentiators of antifungal miconazole activity, Produced by *Beauveria sp.* FKI-1366. II. Structure elucidation. *J. Antibiot. (Tokyo)* **57**, 117–124 (2004).
34. Arrowsmith, C.H. *et al.* The promise and peril of chemical probes. *Nat. Chem. Biol.* **11**, 536–541 (2015).
35. Jacinto, E. & Hall, M.N. Tor signalling in bugs, brain and brawn. *Nat. Rev. Mol. Cell Biol.* **4**, 117–126 (2003).
36. Bruno, V.M. & Mitchell, A.P. Regulation of azole drug susceptibility by *Candida albicans* protein kinase CK2. *Mol. Microbiol.* **56**, 559–573 (2005).
37. Egner, R., Rosenthal, F.E., Kralli, A., Sanglard, D. & Kuchler, K. Genetic separation of FK506 susceptibility and drug transport in the yeast Pdr5 ATP-binding cassette multidrug resistance transporter. *Mol. Biol. Cell* **9**, 523–543 (1998).
38. Ma, J.F., Grant, G. & Melera, P.W. Mutations in the sixth transmembrane domain of P-glycoprotein that alter the pattern of cross-resistance also alter sensitivity to cyclosporin A reversal. *Mol. Pharmacol.* **51**, 922–930 (1997).
39. Katzmann, D.J., Epping, E.A. & Moye-Rowley, W.S. Mutational disruption of plasma membrane trafficking of *Saccharomyces cerevisiae* Yor1p, a homologue of mammalian multidrug resistance protein. *Mol. Cell. Biol.* **19**, 2998–3009 (1999).
40. Roemer, T. *et al.* Confronting the challenges of natural product-based antifungal discovery. *Chem. Biol.* **18**, 148–164 (2011).
41. Piper, P.W. & Millson, S.H. Spotlight on the microbes that produce heat shock protein 90-targeting antibiotics. *Open Biol.* **2**, 120138 (2012).
42. Xu, Y. *et al.* Biosynthesis of the cyclooligomer depsipeptide beauvericin, a virulence factor of the entomopathogenic fungus *Beauveria bassiana*. *Chem. Biol.* **15**, 898–907 (2008).
43. Lehár, J. *et al.* Synergistic drug combinations tend to improve therapeutically relevant selectivity. *Nat. Biotechnol.* **27**, 659–666 (2009).
44. Kumar, R., Musiyenko, A. & Barik, S. *Plasmodium falciparum* calcineurin and its association with heat shock protein 90: mechanisms for the antimalarial activity of cyclosporin A and synergism with geldanamycin. *Mol. Biochem. Parasitol.* **141**, 29–37 (2005).
45. Barquilla, A., Crespo, J.L. & Navarro, M. Rapamycin inhibits trypanosome cell growth by preventing TOR complex 2 formation. *Proc. Natl. Acad. Sci. USA* **105**, 14579–14584 (2008).
46. Wang, Q. & Xu, L. Beauvericin, a bioactive compound produced by fungi: a short review. *Molecules* **17**, 2367–2377 (2012).

Acknowledgments

We thank the Donnelly Sequencing Centre for whole genome sequencing; the 2013 MGY360H1 class for performing and analyzing whole-genome sequencing data for a

© 2016 Nature America, Inc. All rights reserved.

subset of the resistant mutants in the ABC16 background; D. Kim for assistance with genome sequencing analysis of the resistant mutants in the *yor1Δ* background; and all members of the Cowen lab for discussions. T.S.-G. is supported by the Ontario Graduate Scholarship and University of Toronto Open Fellowship. L.E.C. is supported by the Canadian Institutes of Health Research (CIHR) Operating Grants (MOP-86452 and MOP-119520), the Natural Sciences and Engineering Research Council (NSERC) of Canada Discovery Grants (06261 and 462167), an NSERC E.W.R. Steacie Memorial Fellowship (477598), and a Canada Research Chair in Microbial Genomics and Infectious Disease. J.H. is supported by the DUKE PO1 (AI104533-01) and RO1 (AI112595-02) for antifungal drug discovery. Y.-S.B is supported by the General International Collaborative R&D program funded by Ministry of Trade, Industry and Energy (MOTIE) in Republic of Korea (N0001720). A.A.L.G. is supported by US Institutes of Health Grants (R01 CA090265 and P41 GM094060). A.-C.G. is supported by a CIHR Foundation Grant, Genome Canada Genomics Innovation Network (GIN) Node and Technical Development Grants, and a Canada Research Chair in Functional Proteomics. J.-P.L was supported by a postdoctoral fellowship from the CIHR and by a TD Bank Health Research Fellowship at the Lunenfeld–Tanenbaum Research Institute. P.C. is supported by the Italian Government (FA). F.T. is supported by a postdoctoral fellowship from MIUR.

Author contributions

L.E.C. and T.S.-G. conceived of and designed the study. T.S.-G. designed and performed selection experiments, drug-susceptibility assays, qRT-PCR, β-galactosidase activity assays, and western blots. R.A. and C.N. analyzed whole-genome sequencing data for a subset of the beauvericin-resistant strains in the ABC16 background. F.P.R. analyzed whole-genome sequencing data for a subset of the beauvericin-resistant strains in the ABC16 background. D.S. designed and performed the azole accumulation experiment. L.S. and K.D. designed and performed the *in vitro* Pdr5 ATPase and rhodamine 6G transport assays. G.M.K.B.G., E.M.K.W., and A.A.L.G. synthesized the biotinylated beauvericin analog. A.-C.G. and J.-P.L. designed the AP–MS experiment; J.-P.L. performed and analyzed AP–MS data under supervision of A.-C.G. F.T. and P.C. designed and performed CK2 kinase activity assays. R.J.L. and K.N.-S. designed and performed experiments to monitor TORC1 and TORC2 activity via Sch9 and Ypk1 phosphorylation, respectively. Y.-S.B., A.F.A., and J.H. designed the *C. albicans* mouse study; Y.-S.B., A.F.A., S.C.L., T.K., and J.H. performed and analyzed the mouse study. D.A. designed and performed the *C. albicans* biofilm study.

Competing financial interests

The authors declare no competing financial interests

Additional information

Any supplementary information, chemical compound information and source data are available in the online version of the paper. Reprints and permissions information is available online at http://www.nature.com/reprints/index.html. Correspondence and requests for materials should be addressed to L.E.C.

© 2016 Nature America, Inc. All rights reserved.

ONLINE METHODS

Ethics statement. *Mouse model of C. albicans disseminated infection.* All procedures for animal research were approved by the Institutional Animal Care and Use Committee (IACUC protocol A114-14-05) at Duke University according to the guidelines of the Animal Welfare Act, The Institute of Laboratory Animal Resources Guide for the Care and Use of Laboratory Animals, and Public Health Service Policy.

Rat central venous catheter model. The studies were approved by the University of Wisconsin IACUC and were completed in compliance with associated ethical regulations.

General culturing conditions. All strains and plasmids used in this study are listed in **Supplementary Tables 1** and **2**, respectively. Strain and plasmid construction procedures are described in **Supplementary Note 2**. *S. cerevisiae*, *C. albicans*, and *C. neoformans* strains were maintained on solid yeast extract peptone dextrose medium (YEPD, 2% peptone, 2% dextrose,1% yeast extract, and 2% agar). The *A. fumigatus* strain was maintained on solid potato dextrose medium at 35 °C. Unless otherwise stated, *S. cerevisiae*, *C. albicans*, and *C. neoformans* strains were grown overnight to saturation at 30 °C in YEPD with continuous agitation. All strains were archived in 25% glycerol and maintained at −80 °C.

Drug susceptibility and checkerboard assays. For evaluating drug combination efficacy against a variety of fungal species we used azole Etest strips (fluconazole and voriconazole, Biomerieux). Hemacytometer counts were used to measure cell densities of *S. cerevisiae*, *C. albicans*, and *C. neoformans* overnight cultures and *A. fumigatus* conidia suspensions in 1× PBS. ~1×10^6 cells or conidia were plated on YEPD with or without 20 μg/ml beauvericin (Cedarlane, Cayman Chemical Co.) before application of azole Etest strips. Isolates were incubated at 30 °C, except for *A. fumigatus* at 35 °C, and plates were photographed after 48 h.

Antifungal-resistant phenotypes were also evaluated by broth microdilution MIC testing in 96-well, flat-bottom microtiter plates (Sarstedt), as previously described[9]. Fluconazole (Sequoia Research Products) was dissolved in sterile ddH_2O, beauvericin in 100% methanol, cycloheximide (AG Scientific Inc.) in sterile ddH_2O, rhodamine-6G (Sigma-Aldrich) in sterile ddH_2O, geldanamycin (Invitrogen) in DMSO, and cyclosporin A (Calbiochem) in DMSO. Assays were setup in a total volume of 0.2 ml/well with two-fold serial dilutions of compounds, as indicated. All wells were inoculated with ~1×10^3 cells/ml from saturated overnight cultures. Plates were wrapped in foil and incubated at 30 °C for the amount of time indicated. Growth was quantified by measuring the optical density (OD) at 600 nm using a spectrophotometer (Molecular Devices) and correcting for media background. All strains were assessed in biological triplicate experiments with technical duplicates. Growth was normalized to untreated controls and plotted as a heat map using Java TreeView 1.1.6r4.

Dose-response matrixes (checkerboard assays) were performed in a similar manner to the broth microdilution MIC testing. Here, two-fold serial dilutions of beauvericin were prepared along the *y* axis and two-fold serial dilutions of either fluconazole or rapamycin (in DMSO, Bioshop Canada Inc.) along the *x* axis. To evaluate cidality of the drug combinations, we used a 96-well replicator tool to transfer cells onto solid, rich medium (YEPD) containing no compound. Plates were photographed after 24 h incubation at 30 °C.

Selection experiments. To select for fluconazole resistance, overnight cultures of wild-type *C. albicans* (SN95) were grown in YEPD at 30 °C and cell density was quantified by hemacytometer counts. ~1×10^5 cells were plated on YEPD or on YEPD containing fluconazole (32 μg/ml), beauvericin (20 μg/ml), or both. Experiments were performed in biological duplicates; plates were incubated at 30 °C for five days and photographed each day.

To select for beauvericin resistance, overnight cultures were grown in YEPD at 30 °C and cell densities were quantified by hemacytometer counts. ~1×10^8 cells were plated on YEPD agar (ABC16 or *yor1Δ*) containing 100 μg/ml of beauvericin. As a control, ~1×10^8 cells were plated on YEPD containing methanol. No growth defect was observed in comparison to media without methanol. The selection experiment with the ABC16 strain was performed once, while the selection experiment with the *yor1Δ* strain was done in biological triplicates.

Whole-genome sequencing. Saturated overnight cultures of the ABC16 and *yor1*Δ parental strains and beauvericin-resistant mutants in each background were grown in 50 ml of YEPD and pelleted at 3,000 r.p.m. for 5 min followed by flash freezing using liquid nitrogen. Genomic DNA extraction, sequencing library preparation, and analysis were performed as previously described[47]. MuTect (Version 1.1.4) (ref. 48) was used to identify unique mutations in beauvericin-resistant strains. The average coverage of each genome was sufficient for confident variant detection and is listed in **Supplementary Table 3**.

Mutations identified in *CKB1*, *CKB2*, and *PDR5* were validated by Sanger sequencing. Each locus or region flanking mutation(s) was PCR amplified from genomic DNA (gDNA) of the respective resistant strains. Reaction mixtures contained 1× HiFi PCR buffer, 0.2 mM dNTPs, 2 mM $MgSO_4$, 0.4 μM primers, 1 unit of HiFi polymerase, ~100 ng of gDNA, and sterile water up to 50 μl. Cycling conditions were 94 °C, 5 min; 94 °C, 30 s; 55 °C, 45 s; and 68 °C, 1 min for 30 cycles; 68 °C 10 min. PCR products were visually confirmed by gel electrophoresis and purified using a PCR cleanup kit (Sigma). ~100 ng of purified product with 7.14 μM of appropriate oligos were sent for sequencing at the TCAG Sequencing Facility. All primers used are listed in **Supplementary Table 4**. Genome sequencing data can be accessed through NCBI accession SRP071748.

Radiolabeled fluconazole accumulation assay. *S. cerevisiae* (BY4741) and *C. albicans* (SC5314) cells were grown overnight in liquid YEPD medium at 30 °C with constant shaking. Cells were diluted to 1×10^5 cells/ml in 5 ml YEPD and grown for 20 h in the absence or presence of beauvericin (20 μg/ml). In these conditions, recovered cells were still in late log phase. Cells were washed with fresh YEPD and resuspended at 1×10^8 cells/ml. A total of 10 μl of [^{3}H] fluconazole (Amersham) dissolved in ethanol, corresponding to 4.32 nmol with a specific activity of 5×10^6 d.p.m./nmol, was added to each of the 2 ml yeast suspensions. Cells were incubated in duplicate at 30 °C in 15 ml Falcon polypropylene tubes with constant shaking. Samples of 0.2 ml from each tube were withdrawn at different time intervals (0, 10, 20, and 30 min) and were mixed with 0.2 ml of cold YNB medium containing 10 μg/ml unlabeled fluconazole, to dilute the labeled fluconazole, and placed in a Spin-X microfiltration unit (0.45 μm pore size) with a nylon membrane (Costar, Cambridge, Mass.) adapted to a microcentrifuge tube. Cells were separated from aqueous medium by centrifugation at 9,000 r.p.m. for 15 s at 4 °C. Cells were washed with the unlabeled fluconazole-YNB medium three times. Cells were resuspended in 100 μl 0.1 M NaOH for lysis, to which 5 ml liquid scintillation medium was added (Ultima Gold; Packard, Groningen, The Netherlands) and counted with Wallac 1409 scintillation counter. Results were expressed as averages in c.p.m./10^7 cells.

Isolation of Plasma Membranes. Yeast cells (YRE1001 *MATa ura3-52 trp1-1 leu2-3,112 his3-11,15 ade2-1 pdr1-3 pdr5pdr5prom::TRP1*) were cultured to an OD_{600} of 1.5 in YEPD at 30 °C. At this time point, the nitrogen sources were replenished by addition of one 10th volume of 5× YP (50 g/liter yeast extract, 100 g/liter peptone). Cells were harvested at an OD_{600} of 3.5. The isolation of plasma membranes was performed as previously described[49,50].

Rhodamine-6G Transport Assay. Active transport of rhodamine-6G (R6G) was determined according to a standard protocol[49] using a Tecan Infinite 200 PRO reader (Tecan). Isolated plasma membranes (3 μl of a 1mg/ml stock solution) were resuspended in 200 μl of transport buffer (50 mM Hepes, pH 7.0, 5 mM $MgCl_2$, 10 mM NaN_3, and 150 nM R6G) and incubated at 30 °C in a 96-well FIA plate (Greiner). In addition, 1 μl of a serial dilution of a beauvericin stock solution was added. The transport was started by addition of 10 mM ATP and the fluorescence was recorded for 20 min (excitation at 524 nm, emission at 558 nm, number of flashes: 30, integration time 2,000 μs).

ATPase Activity Assay. Oligomycin (OM)-sensitive ATPase activity of Pdr5 in highly enriched plasma membrane was measured by a colorimetric assay and performed in 96-well microtiter plates[50]. 80 μl of the plasma membrane

© 2016 Nature America, Inc. All rights reserved.
npg

doi:10.1038/nchembio.2165

solution (20 µg/ml stock solution) were incubated with 2 mM ATP, 5 mM $MgCl_2$ in 270 mM Tris-glycine buffer (pH 9.5) and 1 µl of the indicated beauvericin concentrations in a total volume of 200 µl. To reduce the background activities, 0.2 mM ammonium molybdate, 10 mM NaN_3 and 50 mM KNO_3 were added, as previously described[51]. In parallel, OM (20 µg/ml) was added to the assay under same conditions. After incubation at 30 °C for 20 min, the reaction was stopped by adding 25 µl of the reaction to 175 µl 40 mM H_2SO_4. The amount of released inorganic phosphate was determined by a colorimetric assay, using Na_2HPO_4 as standard. The difference of both assays corresponds to the OM-sensitive ATPase activity of Pdr5 (ref. 50).

Rhodamine-6G accumulation assay. *S. cerevisiae* wild-type (BY4741), *pdr5*Δ, *yor1*Δ, and beauvericin-resistant mutants *yor1*Δ R1, R2, and R5 were grown overnight in YEPD at 30 °C. Overnight cultures were diluted to an OD_{600} of 0.2 and incubated at 30 °C for 2 h. 1 µg/ml of R6G was added and cultures were incubated for another 30 min at 30 °C. Samples were washed twice with 1× PBS followed by DIC and fluorescence microscopy to monitor R6G accumulation in cells.

CK2 kinase activity assays. Phosphorylation assays were performed in CK2 buffer (50 mM Tris-HCl pH 8, 150 mM NaCl, 10 mM $MgCl_2$) with 0.1 mM ATP at 37 °C, as previously reported[52]. The CK2 α and β subunits (177 nM CK2α, 4.4 nM CK2 $\alpha_2\beta_2$) used were recombinant human subunits purchased from Biaffin. The recombinant His_6-Sic1 protein was expressed and purified from *E. coli* as previously reported[22]. Briefly, His_6-Sic1 was purified on Ni^{2+}/NTA beads, as described (Qia expressionist handbook, Qiagen), and eluted with 100 mM imidazole. Protein concentration was measured using the Bradford method (Bio-Rad protein assay kit, Bio-Rad Laboratories, Hercules, CA, USA). Samples were taken at the indicated time points for western blot analysis to detect Sic-pS201 with anti-Sic1-pSer201 antibody (dilution 1:2,000)[23]. 300 ng of Sic1 protein was loaded for each lane.

The ABC16 strain was grown in YEPD medium until early exponential phase (0.2–0.3 OD/ml) and either left untreated, treated with 50 µg/ml beauvericin for 5 h, or treated with the vehicle control. Then, cells were collected by filtration and immediately frozen at −80 °C. Crude protein extracts were obtained by a standard glass beads method using lysis buffer (50 mM Tris-HCl pH 7.5, 150 mM NaCl, 0.1% NP-40, 10% glycerol) with 1 mM phenylmethanesulfonyl fluoride (PMSF), protease inhibitor mix (Complete EDTA free protease inhibitor cocktail tablets, Roche) and phosphatase inhibitor mix (Sigma).

CK2 activity of crude protein extracts from the ABC16 strain (0.25 µg) and respective resistant mutants were tested using the purified recombinant protein His_6-Sic1 (7.5 µg) as a substrate in a reaction mix containing 10 mM Tris-HCl pH 7.5, 150 mM NaCl, 10 mM $MgCl_2$, 0.1 mM ATP at 30 °C for the indicated time points. 5 µg/ml beauvericin was added to the reaction mix containing protein extract from ABC16 cells previously untreated with beauvericin *in vivo*. CK2 phosphorylation of His_6-Sic1 was analyzed by SDS-PAGE, probed with anti-Sic1-pSer201 antibody and with anti-His probe antibody (1:1,000, Santa Cruz) as control. Densitometric analysis of three independent experiments was performed using ImageJ (NIH, https://rsbweb.nih.gov/ij/).

Affinity purification coupled to mass spectrometry with biotinylated beauvericin. AP–MS was performed in three independent experiments. Experiments 1 and 2 were performed using 0.1% NP-40 buffer, and experiment 3 was performed using 1% Triton X-100 buffer to allow for efficient extraction of membrane proteins. As the AP protocol was optimized, the amount of excess unlabeled beauvericin was increased to enable detection of high-affinity beauvericin targets.

Beauvericin pull-down and sample preparation. Before lysing cells, batches of Dynabeads MyOne Streptavidin C1 (Invitrogen product # 65001, 25 µl per sample) were washed with lysis buffer (50 mM Hepes-NaOH pH 8.0, 300 mM KCl, 2 mM EDTA, 0.1% NP40, 10% glycerol, 1 mM PMSF, 1 mM DTT and Sigma protease inhibitor cocktail, P8340, 1:500) three times before being resuspended in 500 µl of lysis buffer. 18 nmol of biotinylated beauvericin in methanol was then added per sample to the streptavidin bead suspension and allowed to pre-bind the beads until the lysates were ready (~2 h) on a nutator at 4 °C. The beads were washed three times with lysis buffer to remove unbound biotinylated beauvericin before being incubated with lysates. Control experiments were performed in which the biotinylated beauvericin was omitted.

Frozen pellets from 0.66 l (4 l for six samples) of *S. cerevisiae* (BY4741) (OD_{600} 0.8–0.9) were resuspended in 20 ml of lysis buffer, aliquoted in 2 ml tubes containing ~500 µl of 0.5 mm glass beads (BioSpec Products, Inc.) and lysed by bead beating for 4 × 1 min on a vortex. The lysates were then transferred to fresh 15 ml tubes, sonicated for 3 × 30 s (10 s ON, 2 s OFF cycles) at amplitude 0.60 using a Qsonica 125 W sonicator equipped with 1/8" probe to shear DNA. The sonicated samples were put back on ice for at least 1 min in between pulses. 2 µl of benzonase (Sigma-Aldrich, E1014, 250 units/µl) was then added to each sample which was incubated at 4 °C for 1 h to further digest chromatin and reduce the lysates viscosity. Samples were centrifuged at 14,000 r.p.m. for 20 min (4 °C), and the supernatant transferred to fresh tubes containing the immobilized biotinylated-beauvericin. Methanol or unlabeled excess beauvericin in methanol were then added to the appropriate samples. The samples were incubated on a nutator at 4 °C for 2 h. Beads were then pelleted by centrifugation at 1,000 r.p.m. for 1 min using a small table-top microfuge and placed on a cold magnetic rack (placed on ice) to collect the beads on the tubes' sides. The supernatant was removed slowly with a pipette and the beads were resuspended in 3 × 1 ml of cold lysis buffer. The beads were transferred to a fresh 1.7 ml tube and washed two more times with 1 ml of 20 mM Tris-HCl pH 8.0, 2 mM $CaCl_2$. Following the last wash, the samples were quickly centrifuged and the last drops of liquid were removed with a fine pipette.

The dried beads were resuspended in 7.5 µl of 20 mM Tris-HCl (pH 8.0) containing 500 ng of trypsin (Sigma, T7575) and the mixture was incubated at 37 °C with agitation overnight (~15 h). The sample was then magnetized and the supernatant was transferred to a fresh tube. Another 500 ng of trypsin was added (in 5 µl of 20 mM Tris-HCl pH 8.0), and the resulting sample was incubated at 37 °C for 3–4 h without agitation. Formic acid was added to the sample to a final concentration of 2% (from 50% stock solution) and stored at −40 °C until ready for mass spectrometric analysis.

Mass spectrometry analysis. Samples were analyzed on the AB SCIEX 5600 TripleTOF in Data Dependent Acquisition (DDA) mode. Approximately one third of the volume of the digested sample (5 µl) was analyzed using a homemade emitter column (75 µm × 10 cm) using Dr. Maisch Reprosil C_{18} 3 µm material. The column was coupled to a NanoLC-Ultra 1D plus (Eksigent, Dublin, CA) system with 0.1% formic acid in water as buffer A and 0.1% formic acid in ACN as buffer B. Samples were loaded on the column for 10 min at 400 nl/min (2% buffer B). The flow rate was then decreased to 200 nl/min and the HPLC delivered an acetonitrile gradient over 120 min (2–35% buffer B over 90 min, 40–60% buffer B over 5 min, hold buffer B at 80% 5 min, return to 2% B over 5 min and re-equilibrate the column for 15 min at 2% B). The DDA parameters were 1 MS scan (250 ms; mass range 400–1250) followed by up to 50 MS/MS scans (50 ms each). Candidate ions between charge states 2–5 and above a minimum threshold of 200 counts per second were isolated using a window of 0.7 a.m.u. Previous candidate ions were dynamically excluded for 20 s with a 50 mDa window. The resulting .wiff files were saved in our local interaction proteomics LIMS, ProHits[53]. TripleTOF 5600 .wiff files were converted to .mgf format using ProteinPilot software before being saved into ProHits for analysis. The searched database contained the *S. cerevisiae* complement of the RefSeq protein database (version 57; 12044 forward and reverse (decoy) entries searched). Files were then searched with Mascot (version 2.3.02) using the following parameters: one missed cleavage site, methionine oxidation and asparagine or glutamine deamidation as variable modifications. Fragment mass tolerance was ± 0.15 Da (monoisotopic) and precursor ± 40 p.p.m. To identify significant interaction partners from the affinity purification data, the data were subjected to Significance Analysis of INTeractome (SAINT) analysis[54] implemented in ProHits[55] using SAINTexpress[19]. To perform SAINTexpress analysis, samples generated with immobilized biotinylated beauvericin were compared to beads-only controls. Proteins with FDR below or equal to 1% were considered to be statistically significant.

All MS files used in this study were also deposited at MassIVE (http://massive.ucsd.edu). The MassIVE ID is MSV000079376 and the MassIVE link

© 2016 Nature America, Inc. All rights reserved.

for download is http://massive.ucsd.edu/ProteoSAFe/status.jsp?task=b6a17bff626f4ff0b408574c69a68489. The data will remain locked until publication but reviewers can access it using the password "beauvericin".

Quantitative reverse transcription (RT)-PCR. *S. cerevisiae* (BY4741) cultures were grown overnight in YEPD at 30 °C. Overnight cultures were diluted to OD_{600} 0.1 treated with or without 40 μg/ml of beauvericin and grown at 30 °C while shaking to OD_{600} 0.4. 0.2 μg/ml of rapamycin was then added to beauvericin-treated and untreated samples and incubated at 30 °C for another 1 h. Cultures were pelleted, washed, and kept frozen at −80 °C. RNA was isolated using the QIAGEN RNeasy kit and further treated with RNase-free DNase (QIAGEN). AffinityScript Multi Temperature cDNA Synthesis Kit (Agilent Technologies) was used to perform complementary DNA synthesis. PCR was performed using Fast SYBR Green Master Mix (Applied Biosystems) and Bio-Rad CFX384 Real Time System, with the following cycling conditions: 95 °C for 3 min; 95 °C for 10 s; and 60 °C for 30 s, for 40 cycles. qRT-PCR reactions were performed in triplicate for biological duplicate experiments. All primer sequences are listed in **Supplementary Table 4**.

Sch9 and Ypk1 *in vivo* phosphorylation assays. The *yor1* strain was grown overnight in YEPD at 30 °C and diluted to an OD_{600} of 0.1, and 5 ml of culture was treated with appropriate vehicle (methanol) or drug (5 μg/ml beauvericin) at appropriate time points. All samples were collected after 4 h. Cell growth was stopped by adding 100% (w/v) TCA to a final concentration of 6% (v/v). After harvesting, cell pellets were processed for western blotting as previously described[56]. A Licor Odyssey Scanner was used to detect phosphorylated Sch9 (P-Sch9^{T758}), phosphorylated Ypk1 (P-Ypk1^{T662}), total Sch9, and total Ypk1. Monoclonal antibodies against P-Sch9, P-Ypk1, and total Sch9 were used, and a commercially available antibody from Santa Cruz (yN-20) was used for total Ypk1 detection. Secondary IRDye antibodies from Li-Cor Biosciences were used for primary antibody detection.

β-galactosidase assays. Strains harboring a 4xCDRE-*lacZ* construct were cultured in the absence or presence of 64 μg/ml fluconazole, and with or without 10 μM geldanamycin, 1 μg/ml FK506 (in DMSO, A. G. Scientific), or 20 μg/ml beauvericin. Strains were grown in synthetic defined (SD) media at 25 °C overnight and diluted the next day to OD_{600} 0.01 ± inhibitors geldanamycin, FK506, or beauvericin. Cultures ± inhibitors were again incubated overnight in s.d. at 25 °C and diluted the next day to OD_{600} 0.3 ± inhibitors in the presence or absence of fluconazole for five hours. Strains harboring the *HSP70-lacZ* construct were treated with 10 μM geldanamycin or 10 μg/ml beauvericin. Strains were grown in YEPD at 30 °C overnight and diluted the next day to OD_{600} 0.01 ± inhibitors geldanamycin or beauvericin. Cultures ± inhibitors were again incubated overnight in YEPD at 30 °C and diluted the next day to OD_{600} 0.2 ± inhibitors for four hours. Post-treatment sample processing and analysis was conducted as previously described[10].

Hog1 western blots. *S. cerevisiae* cultures were grown overnight in YEPD at 30 °C, diluted to OD_{600} 0.1 treated with or without 2.5 μg/ml beauvericin, and grown at 30 °C while shaking to OD_{600} 0.5. 0.7 M NaCl was added to beauvericin-treated and untreated samples, which were incubated at 30 °C for another 30 min. At this point, 1 ml of culture was pelleted at 13,000 r.p.m. for 30 s, resuspended in 2× SDS sample buffer (6× sample buffer: 0.35 M Tris-HCl, 10% (w/v) SDS, 36% glycerol, 5% β-mercaptoethanol, and 0.012% bromophenol blue), boiled at 100 °C for 5 min and centrifuged for 30 s. Proteins were separated by SDS-PAGE using an 8% acrylamide gel. Proteins were electrotransferred to PVDF membranes (Bio-Rad Laboratories, Inc.) and blocked with 5% skimmed milk in phosphate buffered saline (PBS) with 0.1% tween or 5% BSA in tris buffered saline (TBS) with 0.1% tween for phospho antibodies. Blots were probed with p38 MAPK antibody (1:1,000, Cell Signaling Technology) to detect phosphorylated Hog1 levels, Hog1 antibody (1:2,500, Santa Cruz Biotechnology) to detect total Hog1 protein levels, and α-tubulin antibody (1:1,000, AbD Serotec). Band intensities were quantified through ImageJ, and tubulin was used as loading control.

Murine model of disseminated candidiasis. Six to seven week old, female BALB/c (inbred) mice were used, with ten mice per treatment. 5×10^6 cells of wild-type *C. albicans* (SC5314) were used to infect mice via lateral tail vein injection. Infected mice were then treated with vehicle (10% 1:1 Ethanol: Cremophor + 90% PBS), 4 mg/kg beauvericin, 0.5 mg/kg fluconazole, or the drug combination via intraperitoneal (IP) injections. Infected mice were randomly chosen for each group. Treatments were administered 4, 24, 48, 72, and 96 h post infection. No blinding was done. For statistical analysis of survival difference, Log-rank (Mantel-Cox) test was used. Survival data for all of the tested mice were included in the statistical analysis.

Rat central venous catheter model of *C. albicans* biofilm infection. This infection model was conducted as previously described[8]. For drug treatments, 500 μg/ml of fluconazole and 4 μg/ml of beauvericin were used alone or in combination. For scanning electron microscopy, catheter segments were processed as previously described[57]. Following overnight fixation (4% formaldehyde, 1% glutaraldehyde in PBS), catheter segments were washed with PBS and treated with osmium tetroxide (1% in PBS) for 30 min. Drying was accomplished using a series of alcohol washes followed by critical point drying. Catheter segments were mounted and gold coated. Images were obtained with a scanning electron microscope (JEOL JSM-6100) in the high-vacuum mode at 10 kV. The images were assembled using Adobe Photoshop 7.0.1.

47. Hill, J.A., Ammar, R., Torti, D., Nislow, C. & Cowen, L.E. Genetic and genomic architecture of the evolution of resistance to antifungal drug combinations. *PLoS Genet.* **9**, e1003390 (2013).
48. Cibulskis, K. *et al.* Sensitive detection of somatic point mutations in impure and heterogeneous cancer samples. *Nat. Biotechnol.* **31**, 213–219 (2013).
49. Kolaczkowski, M. *et al.* Anticancer drugs, ionophoric peptides, and steroids as substrates of the yeast multidrug transporter Pdr5p. *J. Biol. Chem.* **271**, 31543–31548 (1996).
50. Ernst, R. *et al.* A mutation of the H-loop selectively affects rhodamine transport by the yeast multidrug ABC transporter Pdr5. *Proc. Natl. Acad. Sci. USA* **105**, 5069–5074 (2008).
51. Goffeau, A. & Dufour, J.P. Plasma membrane ATPase from the yeast *Saccharomyces cerevisiae*. *Methods Enzymol.* **157**, 528–533 (1988).
52. Tripodi, F. *et al.* CK2 activity is modulated by growth rate in *Saccharomyces cerevisiae*. *Biochem. Biophys. Res. Commun.* **398**, 44–50 (2010).
53. Liu, G. *et al.* ProHits: integrated software for mass spectrometry-based interaction proteomics. *Nat. Biotechnol.* **28**, 1015–1017 (2010).
54. Choi, H. *et al.* SAINT: probabilistic scoring of affinity purification-mass spectrometry data. *Nat. Methods* **8**, 70–73 (2011).
55. Choi, H. *et al.* Analyzing protein-protein interactions from affinity purification-mass spectrometry data with SAINT. *Curr. Protoc. Bioinformatics* Chapter 8 Unit8.15 (2012).
56. Urban, J. *et al.* Sch9 is a major target of TORC1 in *Saccharomyces cerevisiae*. *Mol. Cell* **26**, 663–674 (2007).
57. Andes, D. *et al.* Development and characterization of an in vivo central venous catheter *Candida albicans* biofilm model. *Infect. Immun.* **72**, 6023–6031 (2004).

© 2016 Nature America, Inc. All rights reserved.

doi:10.1038/nchembio.2165